WEP Warwick Evans Publishing

International Journal of Materials Science and Technology Studies

ISSN: 3006-7693 (Print), ISSN: 3006-3744 (Online) | Volume 4, Number 1, Year 2025
DOI: https://doi.org/10.62051/ijmsts.v4n1.02
Journal homepage: https://wepub.org/index.php/IJMSTS/index

The Performance of Recycled Fine Aggregate Foamed Concrete Incorporating Ground Granulated Blast Furnace Slag-Steel Slag

Bo Zhang

School of Civil Engineering, Henan Polytechnic University, Jiaozuo, 454000, China
212308020084@home.hpu.edu.cn

ABSTRACT

To address the low utilization rates of discarded concrete and industrial solid wastes, this study developed a novel foam concrete (FC) incorporating ground granulated blast furnace slag (GGBS), steel slag (SS), and cement as binders, with natural river sand blended with carbonized recycled fine aggregate (CRFA) as fine aggregates, and reinforced with modified basalt fiber (MBF). FC can be used to backfill voids in underground projects, which not only reduces the overall weight of the building, but also insulates and saves energy. Initially, a univariate experiment determined the optimal CRFA replacement rate and MBF content. Subsequently, the effects of GGBS and SS on the mechanical and physical properties of FC were investigated. Scanning electron microscopy (SEM) and X-ray diffraction (XRD) analyses revealed a synergistic hydration mechanism between GGBS and SS. The results showed that a 20% CRFA replacement and 4 kg·m-3 MBF produced maximum compressive and flexural strengths while reducing thermal conductivity. Additionally, the simultaneous addition of GGBS and SS decreased CH content and refined the pore structure, yielding a more uniform distribution with fewer connected pores. When both GGBS and SS were incorporated at a 20% replacement level, the 28-day compressive and flexural strengths peaked, and thermal conductivity decreased with increasing slag ratios. These findings confirm the synergistic hydration phenomenon of GGBS and SS and offer theoretical guidance for the engineering application of FC.

KEYWORDS

Foam concrete; Steel slag; Blast furnace slag; Recycled aggregate; Basalt fiber

1. INTRODUCTION

FC is a lightweight, highly porous concrete renowned for its exceptional soundproofing, fire resistance properties, and thermal insulation. These attributes make it widely applicable in building fill, insulation layers, and structural components [1, 2]. However, the low strength and susceptibility to cracking of FC limit its applications [3]. Concurrently, mounting volumes of waste concrete and industrial residues including SS and GGBS continue to accumulate persistently, presenting escalating disposal complexities. Additionally, the demand for natural construction materials is on the rise [4, 5]. Replacing natural aggregate (NA) with Recycled aggregate (RA) extracted from waste concrete, along with the incorporation of SS and GGBS into concrete, facilitates resource recycling, decreases the use of natural materials, and protects the environment.

However, RA has higher water absorption and lower strength compared to NA, which negatively impacts the performance of recycled concrete (RC), thereby limiting its engineering applications [6]. Carbonation treatment can densify the mortar adhered to RA, increasing apparent density while

reducing porosity and water absorption [7, 8]. Shi et al. [9] observed that carbonation effectively reduces the porosity in the interfacial transition zone (ITZ), thereby increasing its microhardness. The variant with carbonated recycled aggregate (CRA) showed a 16.7% enhancement in 28-d compressive strength compared to concrete utilizing untreated RA [9]. Additionally, fiber reinforcement provides an effective means to further improve the toughness and strength of concrete [10]. Basalt fiber (BF), as an inorganic fiber, exhibits high elastic modulus, exceptional tensile strength, excellent heat resistance, ease of processing, and environmental and economic benefits [11, 12]. Gencel investigated the effects of BF on FC and found that BF enhanced mechanical performance while increasing the porosity and water absorption of FC [13]. However, the smooth surface of BF hinders its bonding with the matrix [14]. Y.G. et al. reported that HCl modification improves the dispersion of BF in cement paste [14].

Among industrial by-products, GGBS, a residue from iron smelting processes, primarily consists of SiO_2, Al_2O_3, CaO, and MgO, and possesses latent hydraulic activity [15]. Partial replacement of cement with GGBS can reduce CO_2 emissions [16]. GGBS can improve the mechanical strength, fluidity, bonding, heat resistance, and pore structure of FC [17, 18]. Esmaily et al. fabricated geopolymer FC through cement replacement with GGBS, achieving higher compressive strength [19]. Aldea et al. revealed that excessive GGBS replacement reduces compressive strength [20].

SS, an industrial by-product from steel production, primarily contains Si, Ca, Fe, Al, and Mg. With an annual output of over 100 million tons in China, SS has a low utilization rate, making its recycling crucial for mitigating environmental pollution and conserving natural resources [21]. SS can be used as aggregate or cementitious material in concrete, but its low reactivity and slow hydration require activation to enhance its hydration capability [22]. Nunes et al. reported that adding SS to pavements improves their mechanical properties, self-healing ability, and durability [23]. Liao et al. [16] found that SS slows down early hydration of cement, reducing early strength. However, at later stages, the strength exceeds that of ordinary cement [16]. Xiang et al. investigated how SS replacement rate, particle size, and water-to-cement (W/C) ratio affect FC and concluded that the replacement rate of SS has the most significant impact, followed by particle size and W/C ratio [22].

The above findings suggest that SS and GGBS, as industrial by-products, exhibit favorable hydration properties and cost advantages. They can be used as cementitious materials, achieving resource recycling and environmental protection [24]. Hence, combining SS and GGBS offers an effective method to enhance the utilization of SS in concrete. Chinese national standard Ground iron and steel slag (GB/T 28293-2012) specifies the performance indicators of steel-slag powder formulated by mixing SS and GGBS in specific proportions, promoting their application in concrete. Studies have shown that SS and GGBS have a synergistic effect and can partially replace cement clinker to produce concrete [24]. Recent research has utilized various industrial by-products (including phosphorus slag, iron tailings, fly ash, copper tailings, and air-cooled slag) to produce aerated concrete [25]. Research indicates that the binder produced by mixing SS and GGBS in proportion exhibits excellent performance [26]. The combined use of GGBS and SS promotes mutual hydration, resulting in a synergistic effect and superior hardened properties [26]. However, research on using SS and GGBS to prepare aerated concrete remains limited.

In summary, cement was partially replaced by SS and GGBS, river sand was partially replaced by CRFA, and MBF was used as reinforcement to prepare GGBS-SS-BF-RA FC. Through single-variable experiments, the optimal CRA and MBF content were determined. On this basis, experiments were conducted with individual additions of SS and GGBS, as well as their hybrid combination. Through macro-performance testing, this study investigated the effects of GGBS and SS content on the mechanical, physical, and thermal properties of FC. Combined with SEM and XRD microstructure tests, the hydration products and microstructure of FC at different GGBS and SS contents were studied, revealing the synergistic hydration mechanism of GGBS and SS.

2. EXPERIMENTAL OVERVIEW

2.1. Materials

The cement was P.O 42.5 Ordinary Portland Cement produced by Jiaozuo Chiba Cement Co., Ltd., with initial and final setting times of 2.5 and 4 hours, respectively, and its performance indicators meet the requirements of Common Portland Cement (GB 175-2023). Fine aggregate included natural fine aggregate (NFA) and recycled fine aggregate (RFA). NFA, a medium-grained river sand, had a fineness modulus of 2.86. RFA was derived from C40-grade concrete that had been cured for 28 days after casting at the structural testing hall of Henan Polytechnic University. The cured concrete was then crushed and screened using a jaw crusher, and subsequently subjected to carbonation. The physical properties of RFA before and after carbonation are shown in Table 1, while the gradation curves of RFA and river sand are shown in Fig. 1. BF, provided by Haining Anjie Composite Materials Co., Ltd. in Zhejiang Province, measures 12 μm in diameter and 13 mm in length. GGBS was provided by Hengyuan New Materials Co., Ltd., with a particle size of 0.012 mm. SS was supplied by Gongyi Water Treatment Materials Co., Ltd., with a particle size of 0.038 mm. The chemical compositions of SS and GGBS are listed in Table 2, and their XRD patterns are presented in Fig. 2. The foaming agent compound foaming agent, provided by Shandong Meijia New Materials Co., Ltd.. The accelerator is HR type, provided by Sichuan Jianke Huarui Building Materials Co.. The water was tap water from Jiaozuo city.

Table 1. Physical properties of fine aggregate

Aggregate type	Particle size (mm)	Apparent density ($kg \cdot m^{-3}$)	Water absorption (%)	Water content (%)
NFA	0.15-4.75	2763	1.14	1.36
RFA	0.15-4.75	2315	10.51	8.64
CRFA	0.15-4.75	2585	9.38	6.87

Table 2. Chemical composition of GGBS and SS(wt %)

Material	CaO	SiO_2	Al_2O_3	Fe_2O_3	MgO	Na_2O
GGBS	38.25	33.50	14.30	0.45	9.03	0.37
SS	35.40	12.26	6.32	21.74	8.42	0.46

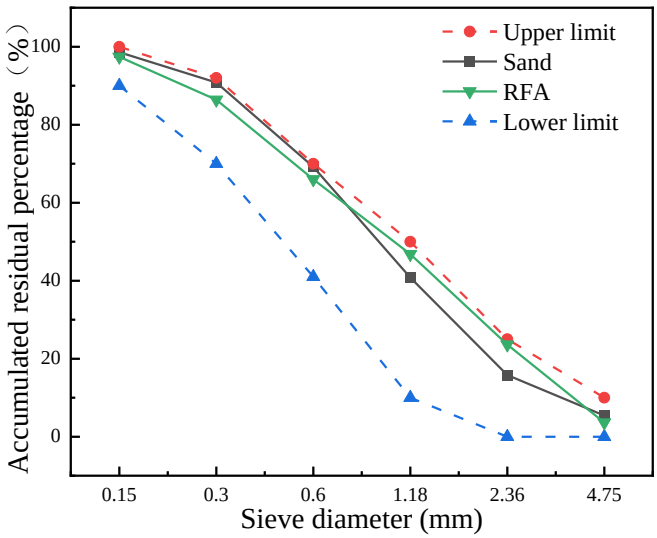

Figure 1. Grading curve of sand and RFA

2.2. Mix Proportion Design

The mix proportion design parameters in this experiment include the dosages of CRFA, MBF, SS, and GGBS, involving multiple variable factors. Therefore, single-variable experiments were first conducted to determine the optimal dosages of CRFA and MBF. Five CRFA replacement rates were designed: 0%, 10%, 20%, 30%, and 40%. The MBF dosages included 0, 2, 4, and 6 $kg \cdot m^{-3}$. Subsequently, single-dosage experiments of GGBS and SS were conducted based on the optimized CRFA replacement rate and MBF dosage. GGBS and SS replaced cement at rates of 0%, 10%, 20%, 30%, and 40%, respectively. Finally, combined experiments with GGBS and SS were carried out, maintaining a constant total replacement rate of 40%. The specific mix proportions are shown in Table 3.

2.3. Specimen Preparation

First, the solid materials were weighed and thoroughly mixed according to Table 3, followed by adding water and stirring for 1 minute to form the cement paste. Next, the foaming agent and water were sequentially added to a bucket at 1:40 and thoroughly mixed using a stirrer. Subsequently, the prepared foam was poured into the cement paste and mixed for a further 3 minutes to produce the foam slurry. Finally, the foam slurry was poured into plastic molds, de-molded after one day, and then cured in a standard chamber at 20 ± 2 °C with relative humidity over 95%.

2.4. Experimental Scheme

2.4.1. Material treatment

(1) Carbonation treatment of RFA

The RFA was placed in a carbonation chamber with a pressure of 0.3 MPa for 24 hours, a CO_2 concentration of 99.9%, a temperature of 20 ± 2°C, and a humidity of 70 ± 5%. Table 2 presents the physical properties of RFA before and after carbonation.

(2) Surface modification of BF

KH560 and PAM was used as a coupling agent to form chemical bonds on the BF surface, improving surface roughness.

2.4.2. Physical properties testing

(1) Porosity testing

The specimens were cut along a plane parallel to the casting surface and then polished. The cut surfaces were photographed with a high-resolution camera, and the images were imported into ImageJ software to measure the porosity of the FC.

(2) Water absorption and dry density testing

The water absorption and dry density test for FC was conducted according to the Foamed concrete (JG/T266-2011).

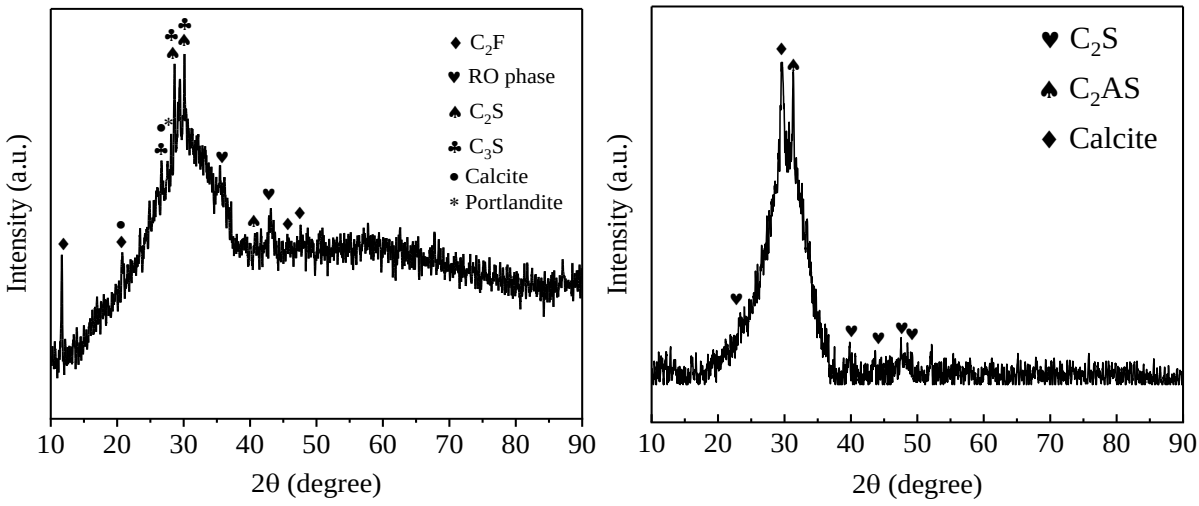

(a) SS (b) GGBS

Figure 2. XRD patterns of SS and GGBS

Table 3. Mix ratio (kg·m^{-3})

Specimen	Water	Cement	GGBS	SS	CRFA	Sand	MBF	Accelerator	Foaming Agent
Control	228.25	415.0	-	-	-	332.0	-	4.15	4.15
R10	228.25	415.0	-	-	33.2	298.8	-	4.15	4.15
R20	228.25	415.0	-	-	66.4	265.6	-	4.15	4.15
R30	228.25	415.0	-	-	99.6	232.4	-	4.15	4.15
R40	228.25	415.0	-	-	132.8	199.2	-	4.15	4.15
BF2	228.25	415.0	-	-	-	332.0	2	4.15	4.15
BF4	228.25	415.0	-	-	-	332.0	4	4.15	4.15
BF6	228.25	415.0	-	-	-	332.0	6	4.15	4.15
G0S0	228.25	415.0	-	-	66.4	265.6	4	4.15	4.15
G1S0	228.25	373.5	41.5	-	66.4	265.6	4	4.15	4.15
G2S0	228.25	332.0	83.0	-	66.4	265.6	4	4.15	4.15
G3S0	228.25	290.0	124.5	-	66.4	265.6	4	4.15	4.15
G4S0	228.25	249.0	166.0	-	66.4	265.6	4	4.15	4.15
G0S1	228.25	373.5	-	41.5	66.4	265.6	4	4.15	4.15
G0S2	228.25	332.0	-	83.0	66.4	265.6	4	4.15	4.15
G0S3	228.25	290.0	-	124.5	66.4	265.6	4	4.15	4.15
G0S4	228.25	249.0	-	166.0	66.4	265.6	4	4.15	4.15
G1S3	228.25	249.0	41.5	124.5	66.4	265.6	4	4.15	4.15
G2S2	228.25	249.0	83.0	83.0	66.4	265.6	4	4.15	4.15
G3S1	228.25	249.0	124.5	41.5	66.4	265.6	4	4.15	4.15

Notes: Control is the normal concrete specimen number, R10 represents 10% of the mass of river sand replaced by RFA, BF2 represents MBF content of 2 kg·m^{-3}, and G1S3 represents 10% and 30% of the mass of cement replaced by GGBS and SS, respectively.

2.4.3. Thermal performance testing

The thermal conductivity was measured following the GB10294-2008 standard for Thermal insulation - Determination of steady-state thermal resistance and related properties - Guarded hot plate apparatus. Specimens sized 300 mm × 300 mm × 30 mm were tested using the DRH-ZD-30 thermal conductivity tester.

2.4.4. Mechanical properties testing

Compressive and flexural strength tests were carried out with a 50 kN electro-hydraulic servo testing machine, following the Chinese standard Foamed Concrete (JG/T266-2011) for test procedures and data analysis.

2.4.5. Microscopic performance testing

Microscopic analysis in the experiment included confocal scanning laser microscope (CSLM), SEM, and XRD. The OLS5000 3D CSLM observed the roughness evolution and three-dimensional morphology, while the S-4800 SEM analyzed the microstructure of the samples. The crystalline composition of the materials was tested using a Nihon Rikaku Rigaku Ultima IV XRD. The CSLM images before and after BF modification are shown in Fig. 3.

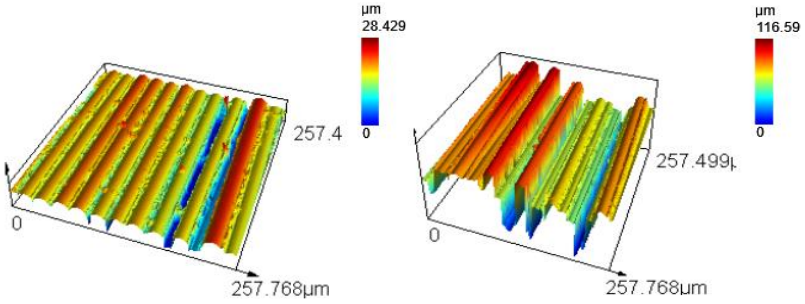

(a)Unmodified BF (b) Modified BF

Figure 3. CSLM 3D topographies of BF before and after modification

As shown in Fig. 3, after modifying the BF surface with a KH560 and PAM mixture, the surface became noticeably rougher, achieving a good modification effect. Therefore, this modified BF was used to prepare the foam concrete.

3. EXPERIMENTAL RESULTS AND ANALYSIS

3.1. Effect of CRFA Replacement Rate

3.1.1. Mechanical properties

Compressive strength and flexural strength are critical mechanical indicators for evaluating the performance of FC, as they directly affect its safety and durability. The physical properties of FC primarily include dry density, porosity, and water absorption. The mechanical and physical properties of FC under various mix proportions are shown in Table 5.

From Table 5, it is evident that variations in the CRFA replacement rate influence the 7-d and 28-d flexural and compressive strengths of recycled foam concrete (RFC) in a similar pattern: initially rising and subsequently declining as the replacement rate increases. The highest compressive strength is observed when the replacement rate reaches 20%. Specifically, at 7 and 28 days, it rises by 2.08% and 1.57%, while the flexural strength improves by 9.52% and 10.71%, respectively. At a 40% CRFA replacement rate, the 7-d strength reductions for compression and flexure were 5.56% and 10.99%, respectively, while the 28-d values declined by 14.29% and 17.86%. These results align closely with those of Kou [27]. The reason is that the surface of the CRFA contains some cement hydration products with certain activity, which can accelerate hydration and enhance the bond between aggregates and the cement matrix during the early curing stage. In this experiment, the recycled micro powder in RFA was not removed. This micro powder can react pozzolanically with the cement paste, filling the cracks in the RFA and thus enhancing its strength when added in small amounts [28]. However, the volume fraction of old mortar within RFC increases as the replacement rate increases. The elevated water absorption of the adhered mortar lowers both the effective W/C ratio and the

workability of RFC. Moreover, the ITZ and defect content in RFC increase [29], leading to a negative impact that outweighs the positive effects, thereby reducing the strength of RFC.

Table 5. Mechanical and physical properties of FC

Specimens	Compressive strength (MPa)		Flexural strength (MPa)		Dry bulk density ($kg \cdot m^{-3}$)	Water absorption (%)	Porosity (%)	Thermal conductivity (W/(m·K))
	7-days	28-days	7-days	28-days				
Control	1.44	1.91	0.21	0.28	818	15.0	30.3	0.234
R10	1.46	1.92	0.22	0.30	810	15.3	30.6	0.232
R20	1.47	1.94	0.23	0.31	807	16.2	31.2	0.228
R30	1.42	1.82	0.20	0.26	793	17.4	32.3	0.230
R40	1.36	1.70	0.18	0.23	786	18.2	33.2	0.226
BF2	1.58	2.22	0.23	0.34	833	16.1	33.3	0.235
BF4	1.72	2.35	0.25	0.40	860	22.5	35.0	0.232
BF6	1.64	2.14	0.29	0.39	838	25.8	35.3	0.229
G0S0	1.76	2.39	0.27	0.42	849	23.6	35.2	0.230
G1S0	1.83	2.87	0.29	0.44	885	20.8	34.1	0.246
G2S0	1.99	3.23	0.31	0.47	904	16.7	33.6	0.253
G3S0	1.81	3.08	0.30	0.46	926	17.3	33.4	0.259
G4S0	1.68	2.83	0.28	0.44	943	18.2	33.2	0.264
G0S1	1.68	3.14	0.24	0.44	887	21.3	34.4	0.263
G0S2	1.60	3.43	0.23	0.49	993	18.8	33.5	0.287
G0S3	1.51	3.15	0.20	0.47	1035	19.5	32.8	0.292
G0S4	1.53	2.97	0.22	0.46	1042	19.7	31.3	0.296
G1S3	1.65	3.16	0.23	0.47	1030	17.8	30.7	0.284
G2S2	1.69	3.58	0.25	0.51	1017	16.2	30.4	0.281
G3S1	1.73	3.42	0.26	0.49	984	17.9	31.4	0.267

Furthermore, it can be observed that flexural strength is more significantly affected by the CRFA replacement rate than compressive strength. This suggests that the replacement rate exerts a stronger impact on flexural performance, a finding also verified by Kumar et al. [30]. The reason is that during flexural failure, microcracks perpendicular to the tensile stress first appear at the edge of the tensile zone in the mid-span, then propagate upward and widen, ultimately leading to tensile failure. This process is more influenced by internal defects. As the replacement rate increases, the ITZ and defect content in RFC increase, causing flexural strength to be more affected by the replacement rate than compressive strength.

3.1.2. Physical properties

The elevated water absorption and porosity of RFA affect the physical characteristics of FC. Table 5 presents the RFC properties at varying replacement rates.

The dry density of FC ranges from 800 ± 20 $kg \cdot m^{-3}$ and gradually declines with a higher replacement rate, aligning with the findings of Pizoń [31]. For instance, at replacement rates of 10%, 20%, 30%, and 40%, the dry density of RFC decreases by 0.98%, 1.34%, 3.06%, and 3.91%, respectively, compared to control. This suggests that the CRFA replacement rate exerts a negligible effect on the dry density of RFC. The reason is that the carbonation treatment of RFA converts CH on the surface into $CaCO_3$, increasing density but remaining slightly lower than NFA. Thus, adding CRFA causes a slight decrease in RFC dry density.

As the replacement rate increases, the dry density decreases while porosity and water absorption increase. For example, at a replacement rate of 20%, the dry density decreases by 1.34%, while water absorption and porosity increase by 8.00% and 2.97%, respectively. This phenomenon, observed by Rodhia et al. [32] and Pizoń et al. [31], is due to the highly porous nature and water absorption of RFA. During production and crushing, the RFA surface retains old mortar and forms microcracks, resulting in significantly higher porosity and water absorption compared to NFA. NFA, being river sand, has relatively smooth particle surfaces, while CRFA has rough and irregular surfaces that tend to form microvoids in concrete. Consequently, the internal structure of RFC becomes looser, and additional water absorption pathways are created, leading to decreased dry density and increased porosity and water absorption.

Table 5 also shows that as the CRFA replacement rate increases, the thermal conductivity of RFC generally decreases (except for R30). At a 40% replacement rate, thermal conductivity reaches its minimum, decreasing by 3.42% compared to the control. This indicates that CRFA can reduce the thermal conductivity of RFC, consistent with the observations of Gencel [33]. The porous nature and lower density of CRFA reduce the dry density of FC and increase the porosity of FC, both of which significantly influence thermal conductivity [34], thereby reducing the thermal conductivity of RFC.

In conclusion, considering the mechanical porosity, thermal conductivity, properties, and dry density of RFC, the optimal CRFA replacement rate is 20%.

3.2. Effect of MBF Content

Table 5 presents the mechanical and physical properties of FC under varying MBF contents.

3.2.1. Mechanical properties

As MBF content rises, both the 7-d and 28-d compressive strengths initially increase and then decrease. The maximum values are observed at an MBF content of 4 $kg \cdot m^{-3}$. When the MBF contents are 2, 4, and 6 $kg \cdot m^{-3}$, the 7-d compressive strengths increase by 9.72%, 19.44%, and 13.89%, while the 28-d values rise by 16.23%, 23.04%, and 12.04%, respectively, compared to the control. These results align with Niaki et al. [35], who reported that the polymer compressive strength of concrete first rose and then declined as MBF content increased, peaking at 1.5 wt% by mass.

The reason is that in an alkaline environment, hydroxyl groups react with the bridging oxygen bonds on the surface of MBF, resulting in improved bonding between MBF and the mortar matrix [13]. Additionally, MBF forms a complex network structure within the matrix, coordinating deformation with the mortar, reducing stress concentration, improving stress distribution, and suppressing crack propagation, thus enhancing strength. However, when excessive MBF is added, the fibers tend to agglomerate, reducing the bonding between MBF and aggregates or cement paste. The 28-d flexural strength increased and then decreased with the increase of MBF dosage, and the 7-d and 28-d flexural strengths increased by 19.05% and 42.86%, respectively, with 4 $kg \cdot m^{-3}$ MBF dosage compared with no MBF dosage, which is consistent with the findings. of Niaki [58].

3.2.2. Physical properties

As MBF content rises, the dry density of FC initially increases and then decreases, reaching a maximum at an MBF content of 4 $kg \cdot m^{-3}$, with an increase of 5.13%. The water absorption of FC increases with rising MBF content, showing increments of 7.33%, 50.00%, and 72.00% at dosages of 2, 4, and 6 $kg \cdot m^{-3}$, respectively. The findings concur with Wang et al. [36], who observed that FC exhibits greater water uptake when a higher proportion of natural fibers is incorporated. This effect is likely due to the expansion of the ITZ within the concrete resulting from fiber addition. Due to surface tension and capillary effects, water penetrates these ITZs, increasing water absorption. The porosity of FC rises with increasing MBF content. When the MBF contents are 2, 4, and 6 $kg \cdot m^{-3}$, the porosity increases by 9.90%, 15.51%, and 16.50%, respectively. Jiang et al. [37] found that incorporating BF into concrete produced a 7.93% elevation in overall porosity measured 28 days later,

accompanied by a larger share of harmful pores. The primary reason is the elevated specific surface area of MBF, which absorbs water upon contact with cement paste [38], leading to increased viscosity and reduced fluidity. This makes it difficult for entrapped air to escape, thereby increasing porosity. When the fiber content is high, fibers tend to agglomerate within the concrete, forming fiber clumps. These regions of fiber agglomeration are poorly filled with paste, resulting in micro-voids and gaps [38].

As the MBF content increases, the thermal conductivity initially increases and subsequently decreases. When the MBF contents are 4 and 6 $kg \cdot m^{-3}$, the thermal conductivity is reduced by 0.85% and 2.14%, respectively. These findings align with those of Zhang et al. [39]. The decrease in thermal conductivity is mainly attributed to the substantially lower thermal conductivity of BF than other concrete materials. Moreover, MBF increases the porosity of FC, and the pores act as effective insulators, further reducing thermal conductivity.

In conclusion, considering both mechanical and physical properties, the optimal MBF dosage is 4 $kg \cdot m^{-3}$.

3.3. Effect of GGBS and SS Content

3.3.1. Mechanical properties

GGBS and SS have good activity and can partially replace cement in concrete preparation. In order to evaluate how GGBS and SS influence the mechanical and physical properties of FC, the replacement rate of CRFA was set at 20%, and the MBF content was 4 $kg \cdot m^{-3}$.

Table 5 demonstrates that GGBS incorporation alone induces an initial enhancement followed by a reduction in both compressive and flexural strengths with increasing dosage, peaking at a 20% replacement level. At a GGBS content of 20%, the compressive strength measured at 28 days improved by 35.15%, while flexural strength saw an increase of 11.90%, aligning with observations reported by Zhang et al. [40]. GGBS demonstrates high reactivity in an alkaline environment, readily interacting with Ca^{2+} within the material to form C-S-H phases, thereby lowering CH content, suppressing the local accumulation of CH, and promoting cement hydration. When the GGBS content is too high, the decline in cement proportion and the rise in inert components limit the hydration reaction, resulting in decreased mechanical properties. Bayraktar et al. [41] observed that increasing GGBS content tends to reduce early concrete strength, potentially due to the particle size of GGBS. Finer GGBS particles demonstrate higher activity and notably enhance the mechanical properties of concrete, especially for low W/C ratio concrete [42]. The above shows that an appropriate amount of GGBS is favorable to improving the mechanical properties of FC, whereas excessive GGBS addition diminishes them.

With the exclusive addition of SS, both the 7-d flexural and compressive strengths of FC generally decreased as SS content increased, except for G0S4. The 28-d flexural and compressive strengths increased initially and then decreased, reaching their maximum values at 20% SS content. At this point, the 28-d flexural and compressive strengths increased by 43.51% and 16.67%, respectively, which aligns with the findings of Ma et al. [43]. This is primarily due to SS hindering C-S-H precipitation [44], along with its higher C_2S content compared to C_3S. [45]. As C_2S hydrates at a slower rate initially but accelerates later, it prolongs the setting time and delays early hydration. Under these factors, the early strength of FC declines, whereas its 28-d strength increases.

Under a fixed 40% combined dosage of GGBS and SS, increasing GGBS or reducing SS leads to higher 7-d compressive and flexural strengths in FC. The compressive and flexural strengths at 28 days initially rise and then decline. When the GGBS and SS contents are both 20%, the 28-d compressive and flexural strengths reach their maximum values, increasing by 49.79% and 21.43%, respectively, compared to G0S0. These results are consistent with Xu et al. [46], who found that compressive and flexural strengths increase initially and then decrease with increasing SS content.

This is because SS contains CaO and MgO, which generate CH during hydration, creating an alkaline environment that promotes the decomposition of GGBS glassy substances and the release of active components. These components generate additional C-S-H gel, while GGBS absorbs Ca^{2+} during hydration, lowering its concentration and further enhancing SS hydration. These findings indicate a synergistic hydration effect between GGBS and SS: SS creates an alkaline environment and supplies Ca^{2+} to facilitate GGBS hydration, while GGBS hydration further promotes SS decomposition, releasing more active components [47]. However, the extent of this synergistic hydration effect depends on the proportion of GGBS and SS. Since SS has lower hydration activity compared to GGBS, an excessive amount significantly slows the reaction rate and the development of hydration products, negatively impacting the mechanical properties of FC, particularly early strength.

3.3.2. Dry density

Dry density is a crucial factor for evaluating the performance of FC as it directly affects its strength and thermal conductivity. In practical engineering applications, the performance of FC can be adjusted by controlling its dry density to meet different requirements. The normalized dry density of FC with varying GGBS and SS contents is shown in Fig. 4.

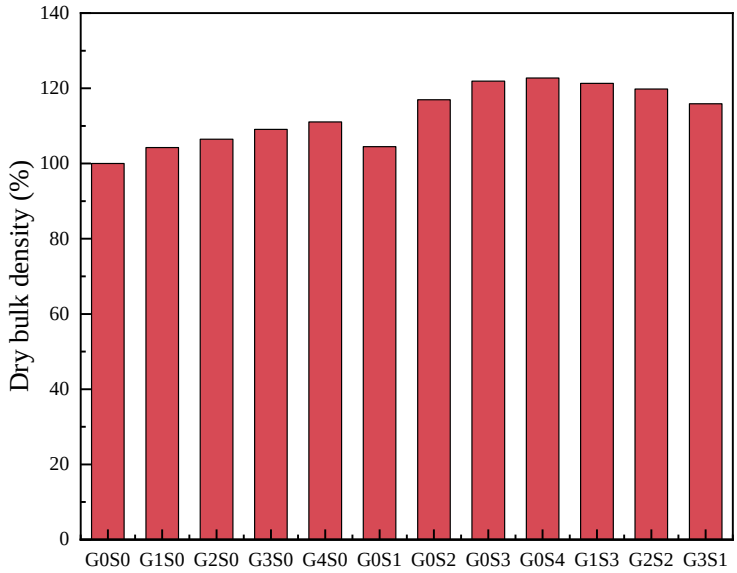

Figure 4. Effect of GGBS and SS replacement rate on FC dry bulk density

As seen in Fig. 4, the dry density of FC increases with the increase in GGBS content. G4S0 shows an 11.07% increase in dry density compared to G0S0. This phenomenon stems from the greater density of GGBS compared to cement, which results in a higher dry density when GGBS replaces cement. In addition, the finer particle size of GGBS contributes to the micro-filling effect and hydration reaction, filling some of the voids and promoting cement hydration to produce more hydration products, thus increasing the dry density.

With increasing SS content, the dry density of FC increases, especially when SS content grows from 10% to 20%, where the dry density rises by 11.95%, followed by a slower growth rate. This is primarily because SS has a higher density than cement, as well as its smaller particle size, which effectively fills voids and enhances material compactness, leading to increased dry density. As the SS content is excessively high, segregation and sedimentation of SS occur, causing slower growth in dry density.

When the total GGBS and SS content is maintained at 40%, increasing GGBS content or reducing SS content leads to a reduction in the dry density of FC. This is because SS has a higher density than GGBS, and with an increase in SS content, the dry density of FC rises.

These results indicate that both GGBS and SS increase the dry density of FC, with SS having a more significant effect.

3.3.3. Water absorption

Water absorption indicates the capacity of FC to take in water when dry, serving as a crucial indicator for assessing its permeability. Fig. 5 displays the normalized water absorption of FC with varying GGBS and SS contents.

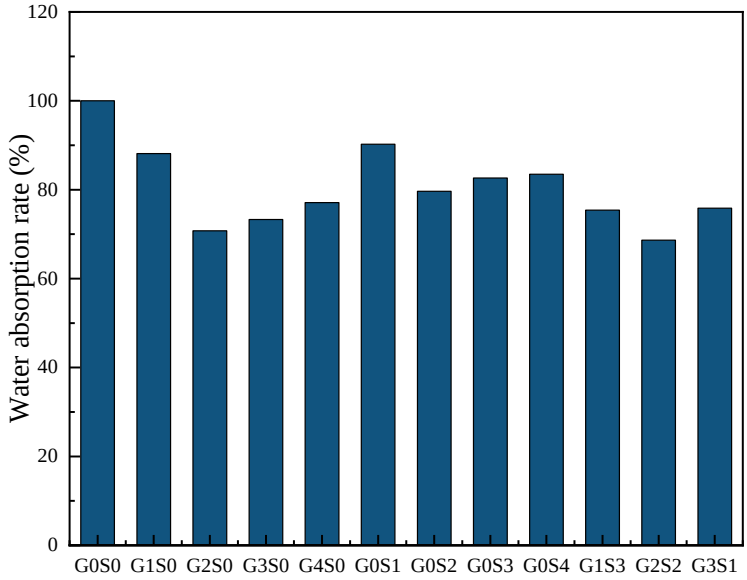

Figure 5. Effect of GGBS and SS replacement rate on FC water absorption

As shown in Fig. 5, when only GGBS is added, the water absorption of FC initially decreases and then increases as GGBS content rises. This aligns with Zhang et al. [29], who found that water absorption and GGBS content exhibit a parabolic relationship, with the lowest water absorption corresponding to the highest compressive strength. At low GGBS contents, the micro-filling and pozzolanic effects of GGBS reduce porosity, thereby decreasing water absorption. As GGBS content continues to increase, the relative reduction in cement content prolongs the setting time, leading to an increased bubble rupture rate, as well as a rise in the content of large and interconnected pores. This results in higher water absorption.

When only SS is added, water absorption follows a similar pattern, initially decreasing and then increasing as SS content rises. This finding is consistent with the results reported by Roslan et al. [48]. The primary reason is that SS possesses significant water absorption, which slows down the hydration process of the cement paste. Unhydrated SS are distributed within the FC matrix, forming weak interface zones that act as channels for water penetration, thus increasing water absorption.

When both GGBS and SS are added, water absorption initially decreases and then increases as GGBS content increases and SS content rises. The lowest water absorption of 16.2% is achieved with G2S2. This is due to the synergistic effect between GGBS and SS [26], where their combined addition produces more hydration products to fill voids, reducing porosity and consequently lowering water absorption. Therefore, the combined addition of GGBS and SS results in lower water absorption compared to their individual addition.

3.3.4. Porosity

Porosity is an important parameter for assessing the internal pore structure of FC, indicating the ratio of pore volume to the total sample volume. It significantly affects the mechanical properties of FC. The pore markers of some specimens for different mixing ratios are shown in Fig. 6, and the porosity is shown in Table 5.

As seen in Table 5, when only GGBS is added, porosity decreases gradually with increasing GGBS content. The lowest porosity of 33.2% is observed at a GGBS content of 40%, representing a 5.68% reduction compared to G0S0. This outcome aligns with the findings of Li et al. [18].

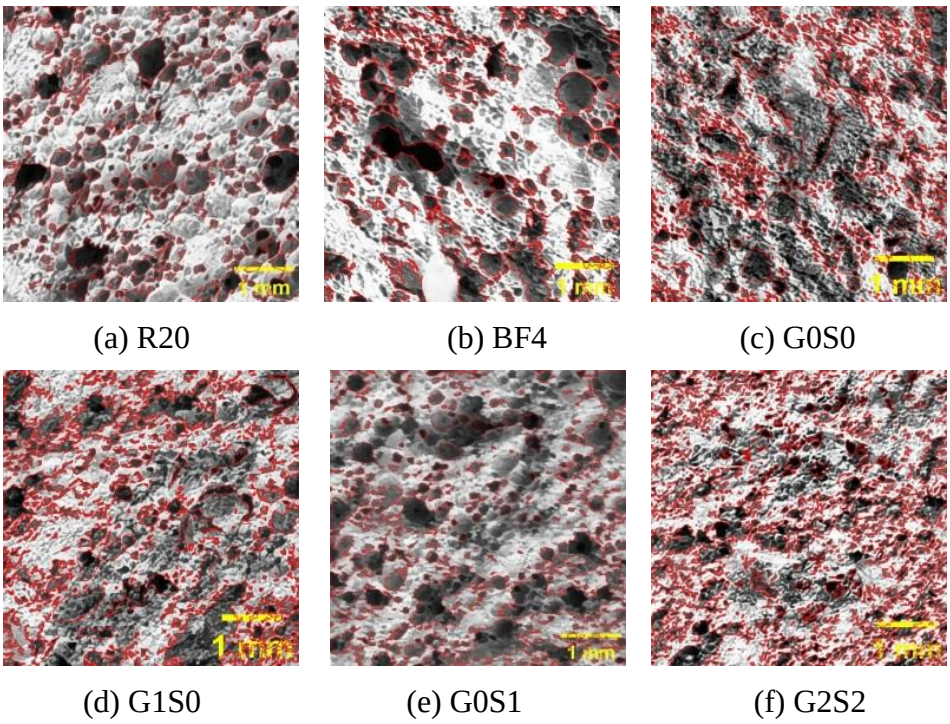

(a) R20 (b) BF4 (c) G0S0

(d) G1S0 (e) G0S1 (f) G2S2

Figure 6. Pore marking diagram of some specimens

When only SS is added, the porosity of FC decreases as SS content increases. The minimum porosity, 31.3%, occurs at 40% SS content, reflecting an 11.08% reduction compared to G0S0. The reduction in porosity of FC is more significant with SS than with GGBS. This is because SS contains some unstable components that expand as the concrete cures, compressing the voids in the matrix. Additionally, SS promotes the formation of aluminate ferrite trisubstituted (Aft), which contains a significant amount of crystalline water. The formation of AFt causes material expansion and fills the voids, further reducing porosity.

When both GGBS and SS are added, the lowest porosity of 30.4% occurs when their contents reach 20% each. During the hydration process, the active particles in SS generate C-S-H gel and CH. However, the CH generated from SS hydration has relatively poor crystallinity and is absorbed by GGBS during the reaction, forming a significant amount of C-S-H gel and AFt. The mutual stimulation and hydration reactions between GGBS and SS effectively reduce porosity.

3.3.5. Thermal conductivity

Thermal conductivity is essential for evaluating the thermal performance of FC, reflecting its ability to transfer heat. The normalized thermal conductivity of FC with varying SS and GGBS contents is shown in Fig. 7.

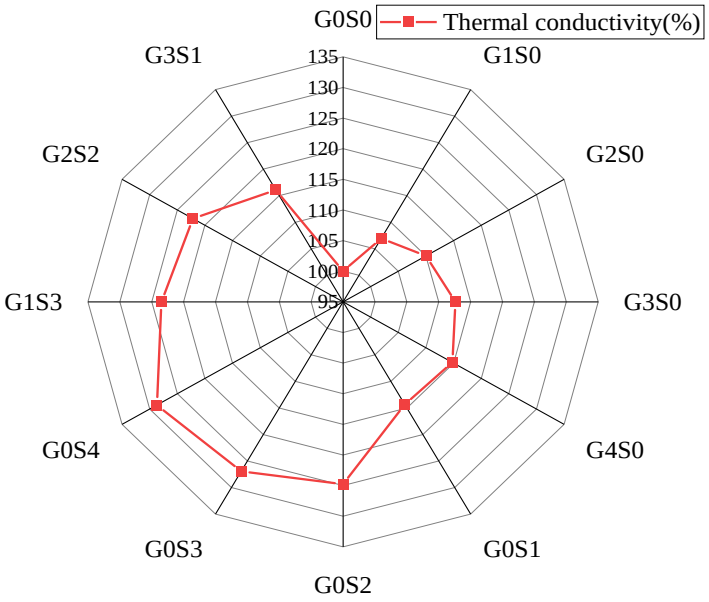

Figure 7. Effect of GGBS and SS on thermal conductivity

As shown in Fig. 7, when only GGBS or SS is added, thermal conductivity increases with increasing GGBS or SS content, with SS having a more significant effect. This finding is corroborated by the study of Okoro and Oyebisi [49]. The hydration products of GGBS or SS fill some of the voids and cracks, making the microstructure of the material denser. When heat transfer occurs, it relies more on pore walls, providing a more efficient heat transfer path and enhancing thermal conductivity. Early hydration of steel slag is slow, easy to rupture the formed bubbles, increasing the matrix compactness, which in turn increases its thermal conductivity.

With combined additions of GGBS and SS, thermal conductivity decreases as the proportion of SS decreases and GGBS increases. For instance, compared to G0S4, G2S2 shows a 5.07% reduction. This phenomenon is also confirmed by the research conclusions of Okoro and Oyebisi [49]. The thermal conductivity is affected by the dry density; since SS density is greater than GGBS, as the ratio of SS to GGBS increases, the dry density increases, leading to an increase in thermal conductivity.

4. SYNERGISTIC HYDRATION MECHANISM OF GGBS AND SS

4.1. XRD Analysis

GGBS and SS possess latent hydraulic activity, and the crystalline types of their hydration products can be analyzed using XRD. The XRD patterns of selected FC samples after 28 days of curing are presented in Fig. 8. Characteristic peaks of SiO_2 can be observed clearly, as it is present in cement, GGBS, and SS. CH primarily originates from cement hydration, although the hydration of GGBS and SS also contributes some CH. $CaCO_3$ results from the reaction between CH and CO_2 and may also come from raw materials exposed to CO_2. Additionally, peaks of AFt, aluminate ferrite monosubstituted (AFm), C_3S, and CAH phases are detected.

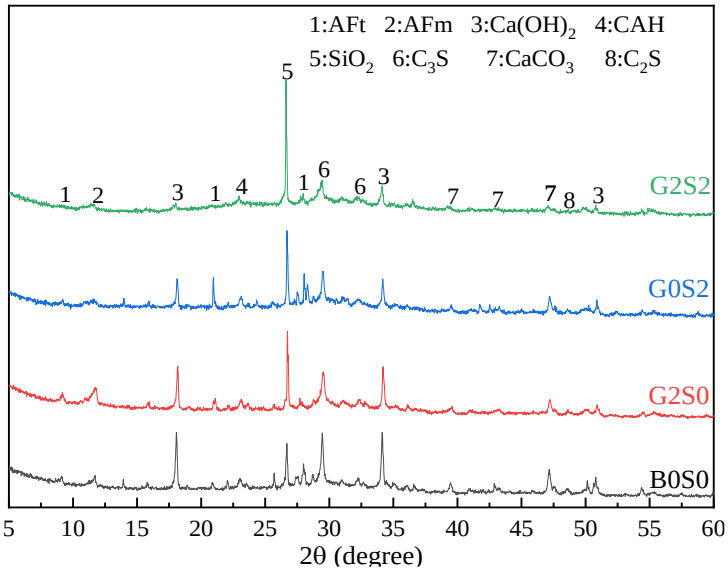

Figure 8. XRD patterns

As shown in Fig. 8, with the addition of GGBS alone, the intensity of C_3S and CH diffraction peaks decreases, while the intensity of AFm diffraction peaks increases. The primary cause is that GGBS lowers the cement content and undergoes secondary hydration with the hydration product CH. The Al_2O_3 content in GGBS is high and highly active. It reacts with Ca^{2+} and SO_4^{2-} generated by cement hydration to form AFm, resulting in an increase in the diffraction peak intensity of AFm. When SS is added alone, the intensity of the CH diffraction peak decreases, the intensity of the AFt diffraction peak significantly increases, and the intensity of the AFm diffraction peak decreases. The reason is that SS contains a certain amount of f-CaO, which provides a certain amount of Ca^{2+} during the hydration process and promotes the formation of AFt. SS enhances the alkalinity of the matrix, and a highly alkaline environment is conducive to the hydration of aluminate minerals and the generation of AFt. Simultaneously, SS exhibits a micro-filling effect, optimizing the pore structure of cement paste and enhancing conditions for AFt formation. Therefore, the addition of SS accelerates the reaction between aluminate minerals and the clinker in cement, thereby promoting the generation of AFt. Free calcium oxide and magnesium ions in SS delay the hydration reaction process, leading to reduced AFm formation.

Compared to the individual addition of GGBS and SS, their combined use results in a continuous decrease in CH diffraction peak intensity, indicating a reduction in CH content. This is because the active components in GGBS and SS undergo secondary hydration with CH, forming C-A-S-H and C-S-H gels while consuming CH. Furthermore, as GGBS and SS replace part of the cement, the cement content is reduced. Since GGBS and SS contain less CaO than cement, the CH content is also reduced.

4.2. Microstructure Analysis

The microstructure of FC incorporating various proportions of GGBS and SS was analyzed using SEM images, as shown in Figs. 9 and 10 at different magnifications.

Without GGBS and SS, a small number of large pores with thinner pore walls are observed in the SEM images. The pore walls appear loose, with some cracks and small pores present. The structure shows more pores, higher porosity, and lower dry density. Additionally, some small pores are seen within the thinner pore walls, even penetrating the walls to form connecting pores. These defects increase stress concentration in weak regions as the stress direction changes, leading to cracks and a decrease in mechanical properties [50]. When SS was added, the thickness of the pore walls increased, resulting in a denser structure compared to G0S0, with fewer cracks. This improvement is reflected in the increased dry density and better mechanical properties. The slower early hydration of SS

extended the setting time, leading to bubble coalescence and the merging of small pores into medium-to-large pores, reducing the number of small pores. After adding GGBS, thicker pore walls are observed, creating a more uniform pore diameter and optimizing the overall pore structure. When GGBS and SS were combined, the pore distribution became more uniform, dominated by small-to-medium pores. The pore walls appeared smooth with fewer connecting pores, which contributed to a higher compressive strength.

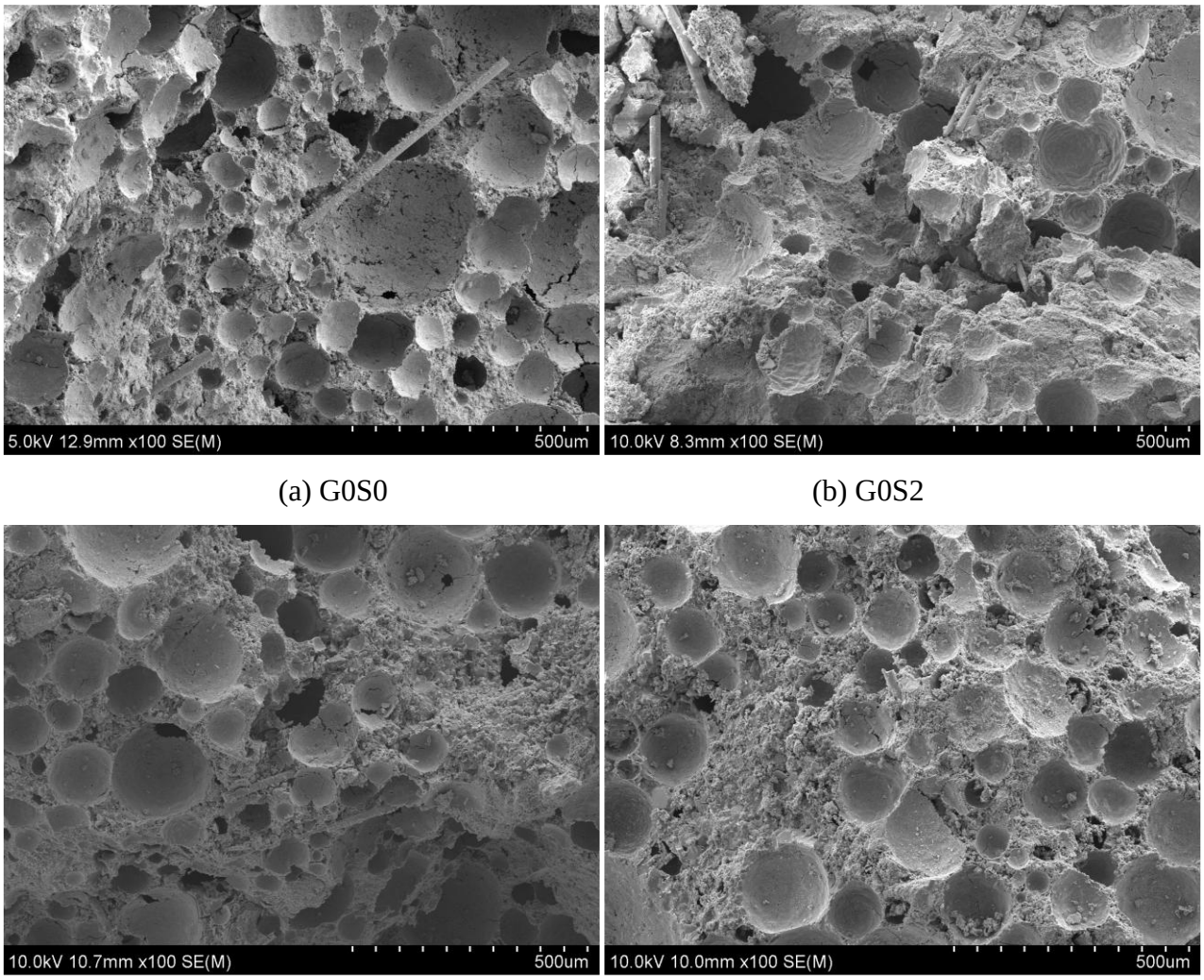

(a) G0S0 (b) G0S2

(c) G2S0 (d)G2S2

Figure 9. SEM images of FC with 100 times magnification

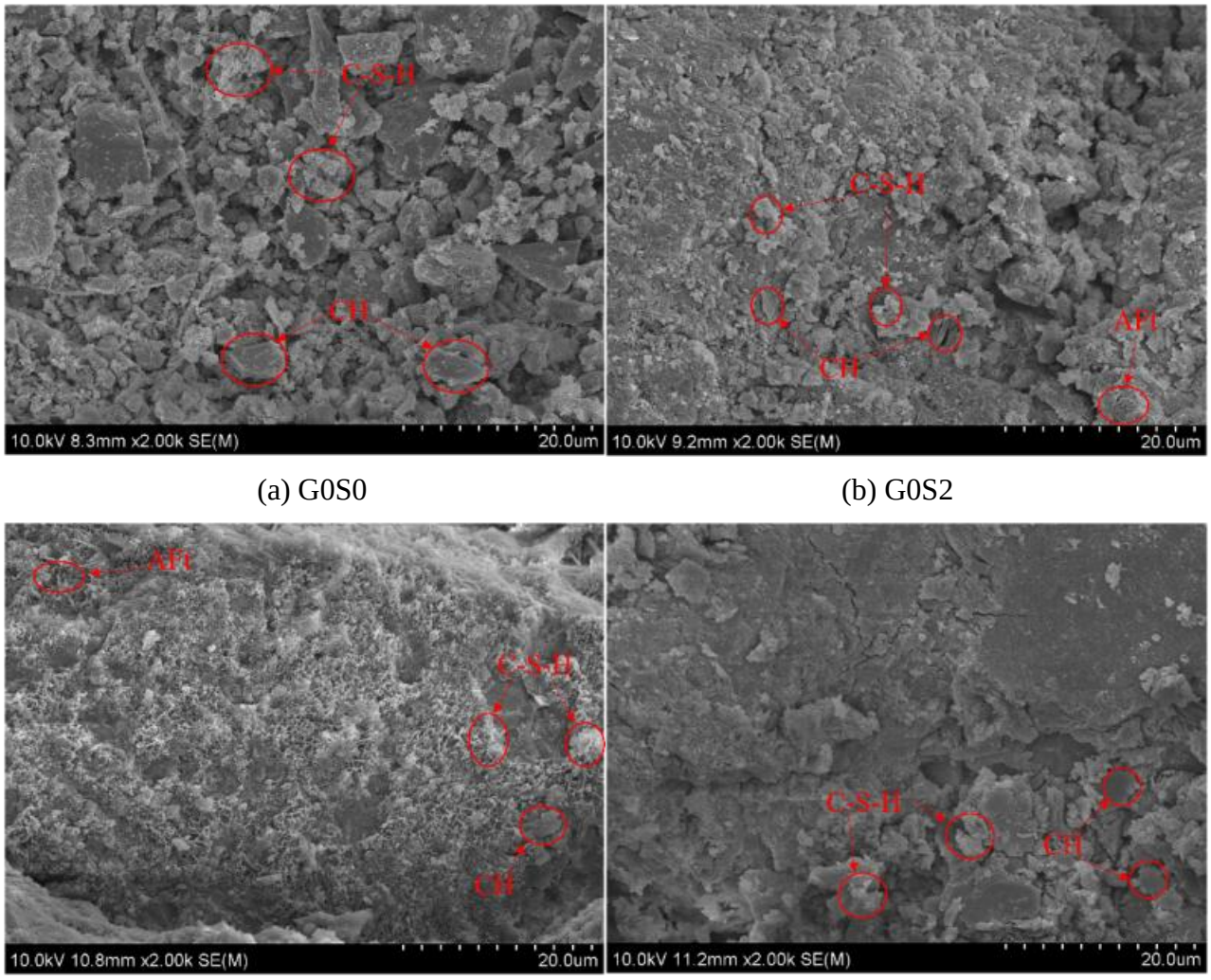

(a) G0S0 (b) G0S2

(c) G2S0 (d) G2S2

Figure 10. SEM images of FC with 2000 times magnification

Flaky CH accompanied by flocculent C-S-H gel is visible in the 2000× SEM image. The FC structure without the addition of GGBS and SS is looser, less dense, and contains more flaky CH, which is consistent with the XRD results and explains the lower strength. After a single addition of GGBS or SS, the content of flaky CH was reduced compared to G0S0, and the structural compactness improved, resulting in an increase in the dry density and strength of the FC. After the combined addition of GGBS and SS, the CH content continued to decrease, and the compactness increased further, leading to an additional improvement in strength.

5. CONCLUSIONS

In this study, the CRFA replacement rate and MBF dosage optimization are first conducted. Based on this, the influences of GGBS and SS on the mechanical, physical, and thermal characteristics of FC are examined. Finally, the mechanism of GGBS-SS synergistic hydration is elaborated through microscopic tests. The main conclusions are as follows:

(1) A novel foam concrete was developed using solid waste and fibers, and the G3S1 meets the requirements of foamed concrete (JG/T266-2011) class A10. It can be used as void backfill in underground engineering with lightweight and heat preservation performance.

(2) Carbonation treatment enhanced the physical properties of RFA. Optimal mechanical performance with concurrent thermal conductivity reduction was achieved in RFC at the 20% CRFA

replacement rate. Therefore, when both strength and thermal performance are taken into account, a 20% replacement rate proves optimal.

(3) The KH560 and PAM mixture exhibited superior modification effects on BF. Incorporating an optimal level of MBF enhanced the mechanical strength and physical performance of FC. Considering both mechanical and physical properties, the optimal MBF dosage is 4 $kg \cdot m^{-3}$.

(4) With single additions of GGBS or SS, an increase in their content led to an initial rise in the 28-d compressive and flexural strength of RFC, followed by a decrease. The maximum 28-d strength was observed at a 20% GGBS or SS replacement rate. With the increase of GGBS or SS proportion, the thermal conductivity and dry density increased, and the porosity decreased.

(5) When GGBS and SS were added together, the 28-d compressive and flexural strengths reached their maximum values when the content of both GGBS and SS was 20%. GGBS and SS increased the dry density of RFC, with SS having a more significant effect. With an increase in GGBS content and a decrease in SS content, water absorption first decreased and then increased. G2S2 showed the lowest porosity and water absorption.

(6) RFC without GGBS and SS contained more flaky CH. After adding SS alone, the pore wall thickness increased, and the number of small pores decreased. After adding GGBS alone, the CH content decreased, and the pore size became more uniform. When GGBS and SS were added together, the CH content decreased, leading to a more uniform pore distribution dominated by small to medium-sized pores with smooth pore walls.

ACKNOWLEDGEMENTS

This work was financially supported by Henan Natural Science Foundation (242300421245), the Henan Provincial Housing and Urban-Rural Construction Science and Technology Project (HNJS-2024-K43), the National Double First Class Discipline Creation and Cultivation Project (AQ20250723, AQ20240729), and the Scientific Research Projects of China Construction Seventh Engineering Division (CSCEC7b-2023-Z-30).

REFERENCES

[1] A. Raj, D. Sathyan, K.M. Mini, Physical and functional characteristics of foam concrete: A review, Constr. Build. Mater. 221 (2019) 787-799, https://doi.org/10.1016/j.conbuildmat.2019.06.052

[2] N. Narayanan, K. Ramamurthy, Structure and properties of aerated concrete: a review, Cem. Concr. Compos. 22 (2000) 321-329, https://doi.org/10.1016/S0958-9465(00)00016-0

[3] S. Feng, Y. Gao, H. Xiao, C. Xue, Influence of fibers and bubble structure on thermal conductivity and mechanical performances of foam concrete, Constr. Build. Mater. 445 (2024) 137956, https://doi.org/10.1016/j.conbuildmat.2024.137956

[4] M. Nedeljković, J. Visser, B. Šavija, S. Valcke, E. Schlangen, Use of fine recycled concrete aggregates in concrete: A critical review, J. Build. Eng. 38 (2021) 102196, https://doi.org/10.1016/j.jobe.2021.102196

[5] Z. Lu, Q. Tan, D. Wang, F. Zhang, J. Lin, Dynamic performance of components constructed from recycled concrete incorporating aggregates modified by accelerated carbonation, J. Build. Eng. 95 (2024) 110273, https://doi.org/10.1016/j.jobe.2024.110273

[6] W. Zuo, X. Zhao, J. Luo, Z. He, J. Zhao, Investigating the impact of carbonation curing concentrations on the mechanical properties and microstructure of recycled concrete, J. Build. Eng. 96 (2024) 110465, https://doi.org/10.1016/j.jobe.2024.110465

[7] B. Zhan, C.S. Poon, Q. Liu, S. Kou, C. Shi, Experimental study on CO2 curing for enhancement of recycled aggregate properties, Constr. Build. Mater. 67 (2014) 3-7, https://doi.org/10.1016/j.conbuildmat.2013.09.008

[8] Y. Li, T. Fu, R. Wang, Y. Li, An assessment of microcracks in the interfacial transition zone of recycled concrete aggregates cured by CO2, Constr. Build. Mater. 236 (2020) 117543, https://doi.org/10.1016/j.conbuildmat.2019.117543

[9] B. Lu, C. Shi, Z. Cao, M. Guo, J. Zheng, Effect of carbonated coarse recycled concrete aggregate on the properties and microstructure of recycled concrete, J. Cleaner Prod. 233 (2019) 421-428, https://doi.org/10.1016/j.jclepro.2019.05.350

[10] M. Iorio, M.L. Santarelli, G. González-Gaitano, J. González-Benito, Surface modification and characterization of basalt fibers as potential reinforcement of concretes, Appl. Surf. Sci. 427 (2018) 1248-1256, https://doi.org/10.1016/j.apsusc.2017.08.196

[11] O.Y. Bayraktar, G. Yarar, A. Benli, G. Kaplan, O. Gencel, M. Sutcu, M. Kozłowski, M. Kadela, Basalt fiber reinforced foam concrete with marble waste and calcium aluminate cement, Struct. Concr. 24 (2023) 1152-1178, https://doi.org/10.1002/suco.202200142

[12] T.M. Borhan, Properties of glass concrete reinforced with short basalt fibre, Mater. Des. 42 (2012) 265-271, https://doi.org/10.1016/j.matdes.2012.05.062

[13] O. Gencel, M. Nodehi, O. Yavuz Bayraktar, G. Kaplan, A. Benli, A. Gholampour, T. Ozbakkaloglu, Basalt fiber-reinforced foam concrete containing silica fume: An experimental study, Constr. Build. Mater. 326 (2022) 126861, https://doi.org/10.1016/j.conbuildmat.2022.126861

[14] Y.G. Deng, B.J. Zhao, T.T. Dai, G.Q. Li, Y. Li, Study on the dispersibility of modified basalt fiber and its influence on the mechanical properties of concrete, Constr. Build. Mater. 350 (2022) 128839, https://doi.org/10.1016/j.conbuildmat.2022.128839

[15] E. Özbay, M. Erdemir, H.İ. Durmuş, Utilization and efficiency of ground granulated blast furnace slag on concrete properties – A review, Constr. Build. Mater. 105 (2016) 423-434, https://doi.org/10.1016/j.conbuildmat.2015.12.153

[16] Y. Liao, G. Jiang, K. Wang, S. Al Qunaynah, W. Yuan, Effect of steel slag on the hydration and strength development of calcium sulfoaluminate cement, Constr. Build. Mater. 265 (2020) 120301, https://doi.org/10.1016/j.conbuildmat.2020.120301

[17] I. Amer, M. Kohail, M.S. El-Feky, A. Rashad, M.A. Khalaf, A review on alkali-activated slag concrete, Ain Shams Eng. J. 12 (2021) 1475-1499, https://doi.org/10.1016/j.asej.2020.12.003

[18] M. Li, H. Tan, X. He, S. Jian, G. Li, J. Zhang, X. Deng, X. Lin, Enhancement in compressive strength of foamed concrete by ultra-fine slag, Cem. Concr. Compos. 138 (2023) 104954, https://doi.org/10.1016/j.cemconcomp.2023.104954

[19] H. Esmaily, H. Nuranian, Non-autoclaved high strength cellular concrete from alkali activated slag, Constr. Build. Mater. 26 (2012) 200-206, https://doi.org/10.1016/j.conbuildmat.2011.06.010

[20] C.-M. Aldea, F. Young, K. Wang, S.P. Shah, Effects of curing conditions on properties of concrete using slag replacement, Cem. Concr. Res. 30 (2000) 465-472, https://doi.org/10.1016/S0008-8846(00)00200-3

[21] H. Li, C. Cui, J. Cai, M. Zhang, Y. Sheng, Utilization of Steel Slag in Road Semi-Rigid Base: A Review, Coatings. 12 (2022), https://doi.org/10.3390/coatings12070994

[22] G. Xiang, D. Song, H. Li, F.E. Jalal, H. Wang, Y. Zhou, Investigation on preparation and compressive strength model of steel slag foam concrete, J. Build. Eng. 72 (2023) 106548, https://doi.org/10.1016/j.jobe.2023.106548

[23] V.A. Nunes, P.H.R. Borges, Recent advances in the reuse of steel slags and future perspectives as binder and aggregate for alkali-activated materials, Constr. Build. Mater. 281 (2021) 122605, https://doi.org/10.1016/j.conbuildmat.2021.122605

[24] C. Ri-gao, W. Zhen-di, W. Ling, Hydration Characteristic and Micro-mrophology of Composite Cementitious Materials with Blast Furnace Slag and Steel Slag, J. Wuhan Univ. Technol. 34 (2012) 25-29.

[25] L. Yang, Y. Yan, Z. Hu, Utilization of phosphogypsum for the preparation of non-autoclaved aerated concrete, Constr. Build. Mater. 44 (2013) 600-606, https://doi.org/10.1016/j.conbuildmat.2013.03.070

[26] J. Zhao, Z. Li, D. Wang, P. Yan, L. Luo, H. Zhang, H. Zhang, X. Gu, Hydration superposition effect and mechanism of steel slag powder and granulated blast furnace slag powder, Constr. Build. Mater. 366 (2023) 130101, https://doi.org/10.1016/j.conbuildmat.2022.130101

[27] S.-C. Kou, C.-S. Poon, Properties of concrete prepared with crushed fine stone, furnace bottom ash and fine recycled aggregate as fine aggregates, Constr. Build. Mater. 23 (2009) 2877-2886, https://doi.org/10.1016/j.conbuildmat.2009.02.009

[28] Y. Lin, T. He, Y. Da, R. Yang, D. Zheng, Effects of recycled micro-powders mixing methods on the properties of recycled concrete, J. Build. Eng. 80 (2023) 107994, https://doi.org/10.1016/j.jobe.2023.107994

[29] C. Liang, H. Ma, Y. Pan, Z. Ma, Z. Duan, Z. He, Chloride permeability and the caused steel corrosion in the concrete with carbonated recycled aggregate, Constr. Build. Mater. 218 (2019) 506-518, https://doi.org/10.1016/j.conbuildmat.2019.05.136

[30] R. Kumar, S.C.B. Gurram, A.K. Minocha, Influence of recycled fine aggregate on microstructure and hardened properties of concrete, Mag. Concr. Res. 69 (2017) 1288-1295, https://doi.org/10.1680/jmacr.17.00030

[31] J. Pizoń, Fresh, Mechanical, and Thermal Properties of Cement Composites Containing Recycled Foam Concrete as Partial Replacement of Cement and Fine Aggregate, Materials. 16 (2023) 7169, https://doi.org/10.3390/ma16227169

[32] R. Rodhia, S.K. Sahdeo, B. Kumar, Optimizing foaming agent concentration and recycled fine aggregate content to enhance mechanical and durable properties of foam concrete mixes, J. Build. Eng. 97 (2024) 110801, https://doi.org/10.1016/j.jobe.2024.110801

[33] O. Gencel, M. Oguz, A. Gholampour, T. Ozbakkaloglu, Recycling waste concretes as fine aggregate and fly ash as binder in production of thermal insulating foam concretes, J. Build. Eng. 38 (2021) 102232, https://doi.org/10.1016/j.jobe.2021.102232

[34] R. Demirboga, A. Kan, Thermal conductivity and shrinkage properties of modified waste polystyrene aggregate concretes, Constr. Build. Mater. 35 (2012) 730-734, https://doi.org/10.1016/j.conbuildmat.2012.04.105

[35] M. Hassani Niaki, A. Fereidoon, M. Ghorbanzadeh Ahangari, Experimental study on the mechanical and thermal properties of basalt fiber and nanoclay reinforced polymer concrete, Compos. Struct. 191 (2018) 231-238, https://doi.org/10.1016/j.compstruct.2018.02.063

[36] X. Wang, Y. Jin, Q. Ma, X. Li, Performance and mechanism analysis of natural fiber-reinforced foamed concrete, Case Stud. Constr. Mater. 21 (2024) e03476, https://doi.org/10.1016/j.cscm.2024.e03476

[37] C. Jiang, K. Fan, F. Wu, D. Chen, Experimental study on the mechanical properties and microstructure of chopped basalt fibre reinforced concrete, Mater. Des. 58 (2014) 187-193, https://doi.org/10.1016/j.matdes.2014.01.056

[38] Y. Wang, A.-H. Kang, Z.-G. Wu, P. Xiao, Y.-F. Gong, H.-F. Sun, Investigation of the basalt fiber type and content on performances of cement mortar and concrete, Constr. Build. Mater. 408 (2023) 133720, https://doi.org/10.1016/j.conbuildmat.2023.133720

[39] X. Zhang, S. Zhang, S. Xin, Performance Test and Thermal Insulation Effect Analysis of Basalt-Fiber Concrete, Materials. 15 (2022) 8236, https://doi.org/10.3390/ma15228236

[40] S. Zhang, X. Qi, S. Guo, L. Zhang, J. Ren, A systematic research on foamed concrete: The effects of foam content, fly ash, slag, silica fume and water-to-binder ratio, Constr. Build. Mater. 339 (2022) 127683, https://doi.org/10.1016/j.conbuildmat.2022.127683

[41] O. Yavuz Bayraktar, G. Kaplan, O. Gencel, A. Benli, M. Sutcu, Physico-mechanical, durability and thermal properties of basalt fiber reinforced foamed concrete containing waste marble powder and slag, Constr. Build. Mater. 288 (2021) 123128, https://doi.org/10.1016/j.conbuildmat.2021.123128

[42] S. Teng, T.Y.D. Lim, B. Sabet Divsholi, Durability and mechanical properties of high strength concrete incorporating ultra fine Ground Granulated Blast-furnace Slag, Constr. Build. Mater. 40 (2013) 875-881, https://doi.org/10.1016/j.conbuildmat.2012.11.052

[43] Y. Ma, C. Zhang, X. Lin, Y. Ye, X. Ye, T. Ji, Bond between alkali-activated steel slag/fly ash lightweight mortar and concrete substrates: Strength and microscopic interactions, Constr. Build. Mater. 449 (2024) 138401, https://doi.org/10.1016/j.conbuildmat.2024.138401

[44] S. Zhuang, Q. Wang, Inhibition mechanisms of steel slag on the early-age hydration of cement, Cem. Concr. Res. 140 (2021) 106283, https://doi.org/10.1016/j.cemconres.2020.106283

[45] D. Fan, C. Zhang, J.-X. Lu, K. Liu, T. Yin, E. Dong, R. Yu, Recycling of steel slag powder in green ultra-high strength concrete (UHSC) mortar at various curing conditions, J. Build. Eng. 70 (2023) 106361, https://doi.org/10.1016/j.jobe.2023.106361

[46] Z. Xu, J. Zhang, J. Zhang, Q. Deng, Z. Xue, G. Huang, X. Huang, Influence of steel slag and steel fiber on the mechanical properties, durability, and life cycle assessment of ultra-high performance geopolymer concrete, Constr. Build. Mater. 441 (2024) 137590, https://doi.org/10.1016/j.conbuildmat.2024.137590

[47] Z.C. Huang, J.C.M. Ho, J. Cui, F.M. Ren, X. Cheng, M.H. Lai, Improving the post-fire behaviour of steel slag coarse aggregate concrete by adding GGBFS, J. Build. Eng. 76 (2023) 107283, https://doi.org/10.1016/j.jobe.2023.107283

[48] N.H. Roslan, M. Ismail, N.H.A. Khalid, B. Muhammad, Properties of concrete containing electric arc furnace steel slag and steel sludge, J. Build. Eng. 28 (2020) 101060, https://doi.org/10.1016/j.jobe.2019.101060

[49] W. Okoro, S. Oyebisi, Mechanical and durability assessments of steel slag-seashell powder-based geopolymer concrete, Heliyon. 9 (2023), https://doi.org/10.1016/j.heliyon.2023.e13188

[50] L. Su, G. Fu, B. Liang, Q. Sun, X. Zhang, Mechanical properties and microstructure evaluation of fly ash - Slag geopolymer foaming materials, Ceram. Int. 48 (2022) 18224-18237, https://doi.org/10.1016/j.ceramint.2022.03.081